Geophysical Research Letters

RESEARCH LETTER
10.1029/2018GL080987

Relative Roles of Preconditioning Moistening and Global Circumnavigating Mode on the MJO Convective Initiation During DYNAMO

Xingchao Chen[1] and **Fuqing Zhang**[1]

[1]Department of Meteorology and Atmospheric Science and Center for Advanced Data Assimilation and Predictability Techniques, The Pennsylvania State University, University Park, PA, USA

Abstract The relative importance of preconditioning moistening and global circumnavigating mode in the convective initiation of the October 2011 Madden–Julian Oscillation (MJO) event observed during the Dynamics of the Madden–Julian Oscillation (DYNAMO) field campaign is investigated using a series of convection-permitting regional model simulations. It is demonstrated that the MJO convective initiation is largely controlled by the global circumnavigating mode at the intraseasonal scales. Rapid moistening closely related to this eastward propagating mode a few days prior to the MJO active phase is crucial to the initiation of deep convection and enhanced rainfall. This moistening process nevertheless cannot be accurately described by the "discharge-recharge" hypothesis, which speculates the importance a gradual moisture buildup over an approximately 2-week period leading to the arrival of the active MJO phase.

Plain Language Summary The Madden–Julian Oscillation (MJO) is a dominant mode of intraseasonal (20–100 days) variability over the tropics. The convective initiation of the MJO corresponds to a transition from predominate shallow clouds to widespread deep convection over tropical oceans. The physical mechanisms related to the MJO convective initiation are still debated. This study uses a series of convection-permitting regional model simulations to show that the gradual buildup of moistening described by the "discharge-recharge" hypothesis cannot accurately describe the convective initiation of the October MJO event observed during the Dynamics of the Madden–Julian Oscillation field campaign. Rapid moistening in the middle troposphere a few days before the MJO active phase is important to the MJO convective initiation. A global eastward propagating circumnavigating mode at the intraseasonal time scales is primarily responsible for the middle-level preconditioning moistening and the eventual convective initiation and enhanced rainfall during the active MJO phase.

Key Points:
- The rapid MJO convective initiation is closely related to the global circumnavigating mode for the October 2011 MJO event during DYNAMO
- Rapid moistening in the middle troposphere a few days prior to the MJO active phase is important to the MJO convective initiation
- It is inaccurate to attribute the convective initiation of the MJO event to the so-called "discharge-recharge" hypothesis

Supporting Information:
- Supporting Information S1

Correspondence to:
X. Chen and F. Zhang,
xzc55@psu.edu;
fzhang@psu.edu

Citation:
Chen, X., & Zhang, F. (2019). Relative roles of preconditioning moistening and global circumnavigating mode on the MJO convective initiation during DYNAMO. *Geophysical Research Letters*, *46*, 1079–1087. https://doi.org/10.1029/2018GL080987

Received 18 OCT 2018
Accepted 7 JAN 2019
Accepted article online 11 JAN 2019
Published online 24 JAN 2019

1. Introduction

The Madden–Julian oscillation (MJO; Madden & Julian, 1971, 1972) is a dominant mode of intraseasonal (20–100 days) variability over the tropics. It has pronounced influences on global weather and climate (e.g., Bergman et al., 2001; Chen et al., 2018; Chi et al., 2015; Lorenz & Hartmann, 2006; Maloney & Hartmann, 2001; Peatman et al., 2014; Rauniyar & Walsh, 2011; Taraphdar et al., 2018; Tyrrell et al., 1996). Though the MJO is a major source of the medium-range predictability for global weather, the physics governing the MJO convective initiation are still debated (Hoskins, 2013; Zhang, 2005). Convective initiation is the transition from predominate shallow clouds (the MJO suppressed phase) to widespread deep convection (the MJO active phase). While evidence suggests that the moistening of the free troposphere is critical to this process (Benedict & Randall, 2007; Johnson et al., 1999; Kikuchi & Takayabu, 2004), both the time scales and the governing mechanisms over this moistening remain debated.

The first mechanism presumes that local gradual moistening and heating processes supported by surface heat and moisture fluxes are responsible for the MJO convective initiation, which is called "discharge-recharge" hypothesis (e.g., Bladé & Hartmann, 1993; Kemball-Cook & Weare, 2001) on a time scale around 2 weeks (Benedict & Randall, 2007). The second mechanism claims that the MJO convective initiation is largely controlled by the external forcing such as the upper-tropospheric global circumnavigating waves (e.g., Ajayamohan et al., 2013; Kikuchi & Takayabu, 2003; Knutson & Weickmann, 1987; Matthews, 2008; Powell & Houze, 2015a) and/or extratropical disturbances that transport energy to equatorial region (e.g., Gahtan & Roundy, 2018; Hsu et al., 1990; Lau & Peng, 1987; Ray & Li, 2013).

There were two strong MJO events comprehensively sampled by the Dynamics of the Madden–Julian Oscillation (DYNAMO) field campaign over the tropical Indian Ocean during 2011/2012 boreal winter (Yoneyama et al., 2013). The first MJO event starts from a suppressed phase in early October without prior MJO event and precedes the initiation of the second MJO event in November. The forecast skill of climate models on the primary October MJO convective initiation is statistically worse than that on the successive November event (Fu et al., 2013; Matthews, 2008). The current study will focus on the October MJO event to identify key physical mechanisms that are responsible for the MJO convective initiation.

DYNAMO sounding observations show that, around 1 week before the October MJO active phase, there is a rapidly local moistening in the middle troposphere that provides a favorable large-scale environment for the subsequent deep convection (Johnson & Ciesielski, 2013; Ruppert & Johnson, 2015). This sounding-observed preconditioning rapid humidification in the middle troposphere is also consistent with the DYNAMO ground-based radar and satellite observations, which show a rapid formation of the widespread moderately deep convection around 3–7 days before the MJO active phase (Powell & Houze, 2013, 2015b). Using a regional convection-permitting simulation, Powell (2016) shows that the moderately deep convection contributes to the humidification below 400 hPa during the rapid transition period. Based on a series of convection-permitting sensitivity experiments, Zhang et al. (2017, Z17 hereinafter) indicate that the convective initiation of the October MJO event over the DYNAMO observation region is largely controlled by the eastward propagating global circumnavigating mode of the MJO upstream of the Indian Ocean. Using the ECMWF reanalysis, Nasuno et al. (2015) demonstrate that the preconditioning moistening processes is dominated by the advection of basic-state moisture by intraseasonal easterly anomalies and of intraseasonal moisture anomalies by the basic-state zonal wind.

In this article, through a set of uniquely designed convection-permitting experiments, we explore the relative roles of preconditioning moistening and global circumnavigating mode on the convective initiation of the October MJO event over the DYNAMO observation region. Key questions addressed by this article concern whether or not the local preconditioning moistening and/or global circumnavigating mode are important to the MJO local convective initiation, if the gradually moistening processes described by the discharge-recharge hypothesis is responsible for the rapid convective initiation of the MJO event and if the circumnavigating mode influences the local preconditioning moistening processes.

2. Experimental Design

The control simulation (CNTL) is the same as in Z17 following Wang et al. (2015, W15) using the Weather Research and Forecasting (WRF) Model (Skamarock et al., 2008) version 3.4.1 at the 9-km grid spacing. Experiment AVG20 is initialized from the CNTL output on 0000 UTC 20 October, with the mixing ratios of water vapor and hydrometeors at all vertical levels between longitudes 65°E and 80°E that are replaced by the mean values of the whole analysis period (from 4 October to 14 November). DRY20 and DRY15 are, respectively, initialized from the CNTL outputs on 0000 UTC 20 and 15 October, with the mixing ratio of water vapor at all vertical levels that are reduced to 50% of its original values and all hydrometeors are removed between longitudes 65°E and 80°E. The initial condition of NOMJO15 is the same as that of DRY15, but the eastward propagating MJO signal is removed from the lateral and lower boundary conditions (Wheeler & Kiladis, 1999). Please refer to supporting information and W15 for model configurations and observational verifications.

3. Results and Discussions

3.1. Evolution of the October MJO Event in CNTL

Figure 1a displays the Hovmöller diagram of daily rainfall and 3-hourly 850-hPa zonal wind averaged between the equator and 5°N from the CNTL simulation. As in W15, CNTL faithfully reproduces the observed initiation, intensity, and eastward propagation of the rainfall associated with the October MJO event. The MJO associated rainfall (or deep convection) begins at ~60°E around 14 October and propagates eastward then with a speed around 5 m/s. The eastward propagation of the MJO associated rainfall is disrupted near the Maritime Continent around 100°E on 5 November. The eastward propagation of the MJO-associated rainfall collocates with a maximum low-level convergence near the leading edge of the westerlies (Figure 1a). The dashed lines in Figure 1a show the region of 70–75°E and 0–5°N, which is a region near both the DYNAMO

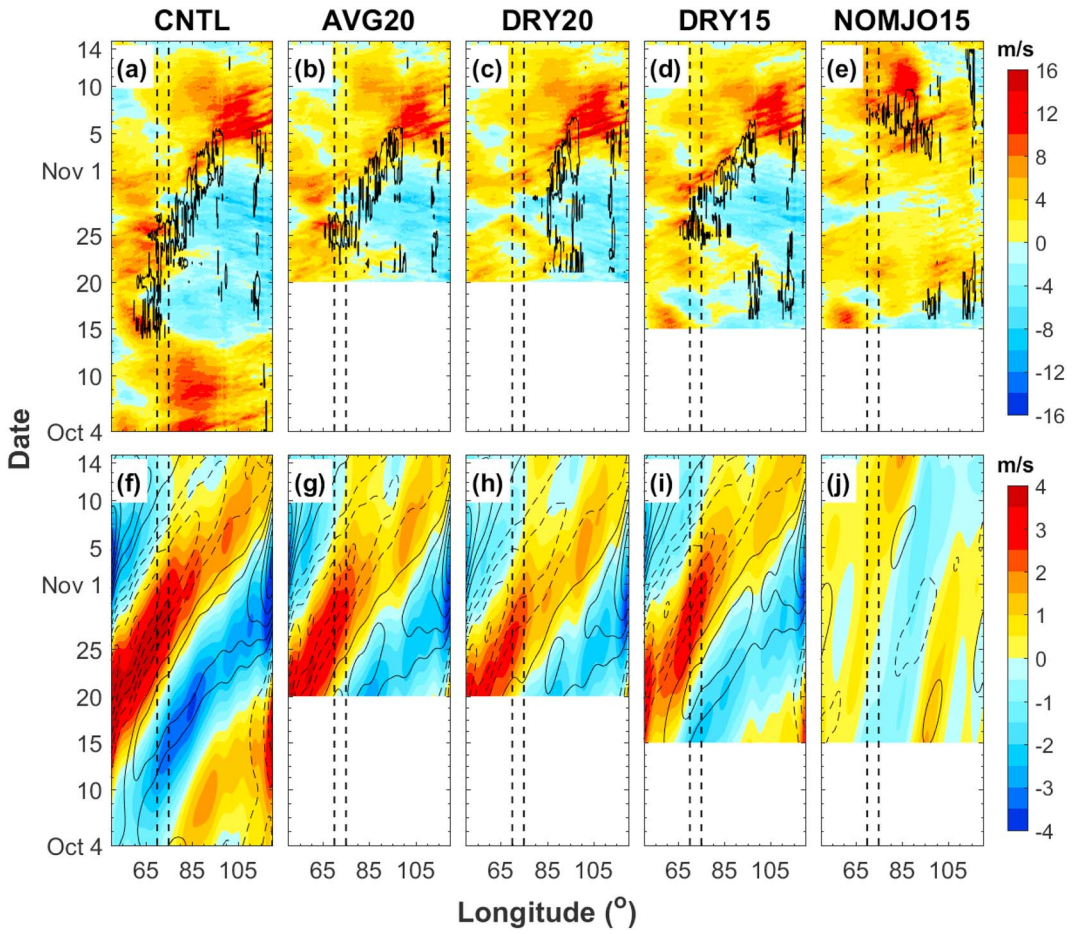

Figure 1. Time-longitude diagram of 3-hourly zonal wind at 850 hPa (shaded) and daily precipitation (contour with a 25 mm/day-interval) from (a) CNTL, (b) AVG20, (c) DRY20, (d) DRY15, and (e) NOMJO15 averaged over the latitude 0–5°N. (f–j) Similar with (a–e) but for the MJO-filtered (20–96 days and wavenumbers 1–9) zonal wind at 850 hPa (shaded) and 200 hPa (contours with an interval at 2 m/s). The solid contours are positive zonal wind, and dashed contours are negative zonal wind. The dashed lines show the SR region (0–5°N, 70–75°E). A 3-day moving average is applied to daily precipitation.

north sounding array where the MJO signal is strongest during the October MJO event (Johnson & Ciesielski, 2013). The following analysis will focus on this special region (SR hereinafter) where the strongest MJO rainfall and organized deep convective activity occur around 26 October.

Figure 1f shows the Hovmöller diagram of the MJO-filtered zonal wind at 200 and 850 hPa averaged between the equator and 5°N from CNTL. As explored in greater details in Z17, the MJO circumnavigating mode and the associated enhanced rainfall propagate from peak at the western boundary of the model domain (around 14 October) to its peak near the east domain boundary (around 5 November) with a speed near 5 m/s. The MJO circumnavigation mode shows a large-scale divergence in the upper troposphere and a large-scale convergence in the lower troposphere near the MJO-associated rainfall region. It shows that this MJO event is induced by a convectively coupled global circumnavigating mode (Z17).

To investigate the preconditioning moistening processes in CNTL, the longitude-height cross sections of daily-averaged relative humidity (RH) averaged over the 0–5°N latitude band are shown in Figures S1 and 2. During 8 October, most Indian Ocean area (from 60°E to 90°E) is still in a suppressed phase with only shallow cloud that occurs below 1.5 km. The middle-to-upper troposphere between 60°E and 90°E is dry with its RH below 50% (Figure S1a). The atmospheric humidity on the east of 90°E is higher than that over the tropical ocean, which may have been moistened by westward propagating inertial gravity waves induced by diurnally driven deep convection over the Maritime Continent. On 10 October, moderately deep convective activities begin to develop between 55°E and 70°E (Figure S1b) and the convective area extends to 85°E on 12

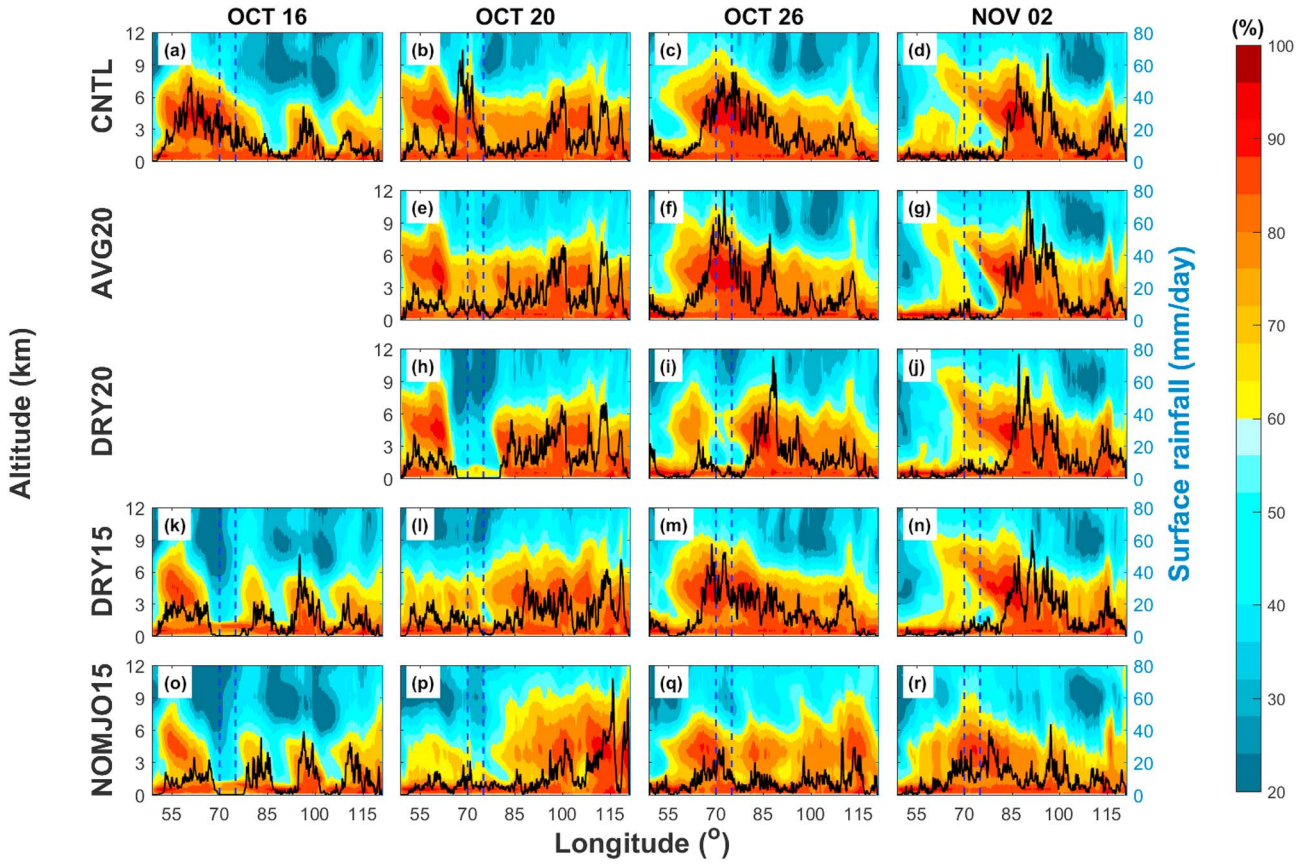

Figure 2. Longitude-height cross sections of daily mean relative humidity (shaded) and longitudinal distributions of precipitation (black line) averaged over the latitude 0–5°N from CNTL experiment on (a) 16 October, (b) 20 October, (c) 26 October, and (d) 2 November. (e–g), (h–j), (k–n), and (o–r) Similar with (a–d) but from AVG20, DRY20, DRY15, and NOMJO15 experiments, respectively. The dashed lines show the SR region (0–5°N, 70–75°E).

October (Figure S1c). The moderately deep convection moistens the middle atmosphere, increases the RH below the melting level (~5 km) to around 70%, and provides a favorable environment for the subsequent deeper convection through overcoming the negative effects induced by the environmental dry air entrainment on the convective updrafts (Hohenegger & Stevens, 2013; Redelsperger et al., 2002; Ruppert & Johnson, 2015). On 14 October, the MJO organized deep convection and enhanced rainfall form near 60°E, which further moisten the upper-level atmosphere above the 0 °C level. Consistent with the Hovmöller diagram shown in Figure 1a, the MJO-associated convection and rainfall propagate eastward then (Figures 2a to 2d), reaching the SR on 26 October (Figure 2c) and arrive ~90°E on 2 November (Figure 2d). The temporal evolutions of RH in CNTL are consistent with the DYNAMO sounding observations (Johnson & Ciesielski, 2013). The time scale of the MJO convective initiation is within a week with a rapid development of moderately deep convection during the transition period as also seen from the DYNAMO radar and satellite observations (Powell & Houze, 2013, 2015b).

3.2. The Importance of Preconditioning Moistening

Figures 1b–1d show the Hovmöller diagram of hourly rainfall and the 850-hPa zonal wind averaged between the equator and 5°N from AVG20, DRY20 and DRY15. In AVG20, after the atmospheric moisture between 65°E and 80°E is replaced with the mean of the whole MJO period, the MJO-associated rainfall weakens from 20 to 22 October and the westerlies able to extend to ~100°E in these 3 days (Figure 1b). However, the MJO-associated rainfall and low-level convergence quickly rebuild starting 23 October in AVG20. Over the SR, the MJO rainfall peak is at similar intensity to that in CNTL during 26 October. In addition, the eastward propagation of the MJO associated rainfall is almost the same as that in CNTL (Figure 1b). The AVG20 experiment indicates that it may only take as short as 3 days for

the required moistening from an otherwise normal tropical moisture environment to deep moist convection during the MJO active phase.

However, such moistening may require a longer period if the prior environment is exceptionally dry. In DRY20, the mixing ratio of water vapor over the SR region at all vertical levels is reduced to 50% of its original values on 00Z 20 October. With a much stronger drying, the enhanced MJO rainfall peak in SR around 26 October does not occur (Figure 1c). Nevertheless, even without the upstream MJO deep convection, the downstream MJO-associated rainfall can still build up around 85°E which subsequently propagates eastward in DRY20.

Even if the prior environment is exceptionally dry, the required local moistening over the SR region may take about a week. In DRY15, when the 50% drying occurs 5 days earlier than DRY20, the MJO rainfall peak over the SR occurs on 26 October. The propagation and intensity of the MJO-associated rainfall after 26 October in DRY15 are also similar to that in CNTL (Figure 1d).

The Hovmöller diagrams of the MJO-filtered zonal wind at 200 and 850 hPa in AVG20, DRY20, and DRY15 are displayed in Figures 1g–1i. The eastward propagation and intensity of the MJO signal in the upper troposphere in all three sensitivity experiments are similar to that in CNTL, which suggests that the weakening of the MJO convection in sensitivity experiments does not influence the upper-level circumnavigating dry mode of the MJO. Nonetheless, in the lower troposphere, the low-level convergences in all these three sensitivity experiments are weaker than that in CNTL. In DRY20, weak convective activity around 65–80°E from 20 October to 26 October may be responsible for a slightly faster eastward extension of the westerlies at 850 hPa (Figures 1c and 1h). In general, we can find that the phase of the upper and lower MJO signals in all three experiments is similar to that in CNTL. It implies that the circumnavigating mode of the MJO is not the result of the MJO convection but serves as the trigger and forcing of the enhanced MJO deep convection, as consistent with findings of Z17.

To further examine the differences in the MJO convective initiation among three sensitivity experiments, the temporal evolutions of humidity averaged along the 0–5°N latitude band from AVG20, DRY20, and DRY15 are compared in Figure 2. In AVG20, the atmosphere between 65°E and 80°E is dryer than that in CNTL on 20 October, especially above the melting level (Figures 2b and 2e). Hence, deep convection over the region is suppressed in AVG20. The surface precipitation is also much weaker with no MJO-associated rainfall peak. However, the humidity below the melting level in AVG20 (Figure 2e) is still much higher when compared to the MJO suppressed phase (Figure S1a), which is similar to the feature of the MJO transition period (Figure S1c). On 26 October, a MJO-associated rainfall peak can be found over the SR with the rainfall intensity close to that in CNTL (Figure 2f). Similar to CNTL, the MJO-associated rainfall in AVG20 propagates to ~90°E on 2 November (Figure 2g).

In DRY20, the humidity between 65°E and 80°E on 20 October (Figure 2h) is much lower than that in AVG20 (Figure 2e), which is similar to the feature of the MJO suppressed phase with the RH in the lower-to-middle troposphere below 50% (Figure S1a). Though the humidity below 1.5 km gradually increases in the next few days, the lower-to-middle troposphere is still very dry on 26 October in DRY20. As a result, there is no MJO rainfall peak over the SR on 26 October (Figure 2i), while a peak can be found near 90°E on 2 November in DRY20 (Figure 2j).

In DRY15, the atmospheric humidity between 65°E and 80°E on 16 October (Figure 2k) is similar to that in DRY20 on 20 October (Figure 2h). During 20 October, moderately deep convective activities are triggered over the SR which moisten the middle troposphere efficiently in DRY15 (Figure 2l). The MJO-associated rainfall peak shows up over the SR on 26 October (Figure 2m) and propagates to near 90°E on 2 November (Figure 2n) in DRY15, which are similar to CNTL.

AVG20 shows that, even the atmospheric humidity is reduced at all vertical levels before the MJO active phase, the MJO-associated rainfall peak can still occur at a same time and location and at a similar intensity. It reflects that the convective initiation of the MJO event is not decided by the gradual moistening in response to stationary surface fluxes described by the discharge-recharge hypothesis. However, the other MJO hypothesis like "wind-induced surface heat exchange" (Emanuel, 1987; Yano & Emanuel, 1991) cannot be ruled out here. The surface heat exchange could be the source of instability for the MJO event. On the other hand, the DRY20 experiment shows that the moistening of the middle troposphere prior to the

active phase is important to the formation of the MJO-associated rainfall and deep convection. DRY15 shows that moderately deep convection triggered before the MJO active phase can efficiently moisten the middle troposphere, and it needs around 5 days to build up the necessarily humidity in the middle troposphere.

3.3. The Importance of Global Circumnavigating Mode

To further elucidate the roles of the global circumnavigating mode on the MJO convective initiation, the MJO signals are filtered out from the lateral and lower boundary conditions in experiment NOMJO15. We can find that the eastward propagating MJO signals of enhanced precipitation (Figure 1e) and MJO-filtered zonal winds (Figure 1j) disappeared in NOMJO15. It further implies that the convective initiation and eastward propagation of the MJO are closely related to the global circumnavigating mode. The result is consistent with findings in Z17. The atmospheric humidity over the SR on 16 October in NOMJO15 is similar to that in DRY15 (Figures 2k and 2o). The humidification of the lower troposphere in the next few days in NOMJO15 is mainly induced by the shallow cumuli (Figure 2p). However, the moistening in the middle troposphere over the SR in NOMJO15 is less efficient than that in DRY15 because less moderately deep convection is triggered in NOMJO15 (Figure 2p). In consequence, there is no clear MJO-associated rainfall peak over the SR on 26 October in NOMJO15 (Figure 2q). On 2 November, the MJO rainfall peak near 90°E is also not clear in NOMJO15. It reflects that even with abundant preconditioning moistening, the global circumnavigating mode is still necessary for the initiation of the MJO deep convection.

The temporal evolutions of RH at 5-km altitude from 16 October to 2 November in CNTL, DRY15, and NOMJO15 are compared in Figure S2. With the deepening of convective activities, the atmospheric humidity at 5-km altitude increases from 16 to 26 October in CNTL (Figures S2a–S2c). On 2 November, the MJO-associated rainfall region shifts to ~90°E and the humidity in the SR begins to decrease (Figure S2d). The daily-averaged RH over the SR at 5-km altitude in DRY15 is lower than 50% on 16 October (Figure S2e). With the development of moderately deep convection, the middle troposphere in the SR is moistened efficiently from 16 to 20 October in DRY15 (Figure S2f). On 26 October, the humidity over the SR at 5-km altitude in DRY15 is similar to that in CNTL (Figure S2g) and a MJO rainfall peak at similar intensity can be found over the SR at this time in DRY15 (Figure 2m). However, the moistening from 16 to 20 October is less efficient in NOMJO15 because of the lack of widespread moderately deep convection (Figures S2i and S2j). The averaged RH over the SR at 5-km altitude is still under 50% on 20 October in NOMJO15 (Figure S2j). As a result, no clear MJO-associated rainfall can be found over the SR on 26 October in NOMJO15 (Figure 2q).

The differences of horizontal winds on 850 hPa between DRY15 and NOMJO15 are shown in Figures S2e–S2h. Results show that filtering out intraseasonal forcing in NOMJO15 leads to subsequent absence of Kelvin waves on the east side of the SR during the convective transition period, which reduces the low-level convergence at the leading edge of the westerlies. The weakening of the low-level convergence leads to the diminishing of widespread moderately deep convection before the MJO active phase in NOMJO15. Filtering out the low-level convergence and upper-level divergence fields associated with the global circumnavigating mode also makes the environment unfavorable for the initiation of deep convection. These results are consistent with the previous studies (e.g., Hohenegger & Stevens, 2013; Ruppert & Johnson, 2015), which indicate that the large-scale dynamical convergence is more important than the local moistening associated with surface fluxes to trigger deep convection over a certain region. Previous studies show that a small reduction in the large-scale subsidence throughout the troposphere may cause an increase of the lapse rate and make the environment more favorable for moderately deep convection (Powell, 2016; Powell & Houze, 2015a). Filtering out of the global circumnavigating mode induces a stronger subsidence in NOMJO15 (not shown here), which contributes to the suppression of the moderately deep convection development from 16 to 20 October in the simulation (Figures S2i and S2j).

Figure 3a shows the time evolutions of the column-integrated frozen moist static energy (MSE $= C_pT + L_vQ_v - L_fQ_i + gz$) averaged over the SR in CNTL, DRY15, and NOMJO15. In CNTL, the column-integrated MSE over the SR increases during 10–15 October. It reaches its maximum (~340×10^7 J/m^2) around 25 October, which corresponds to the MJO active phase over the SR. Consistent with the column-integrated MSE, the vertical-integrated water vapor also increases during 10–15 October and peaks around 25 October (Figure 3b). The changes of the vertical-integrated water vapor are mainly contributed by the changes of the water vapor content above 850 hPa (Figure 3c). During 10–15 October, an enhancement of the low-level moisture convergence associated with the

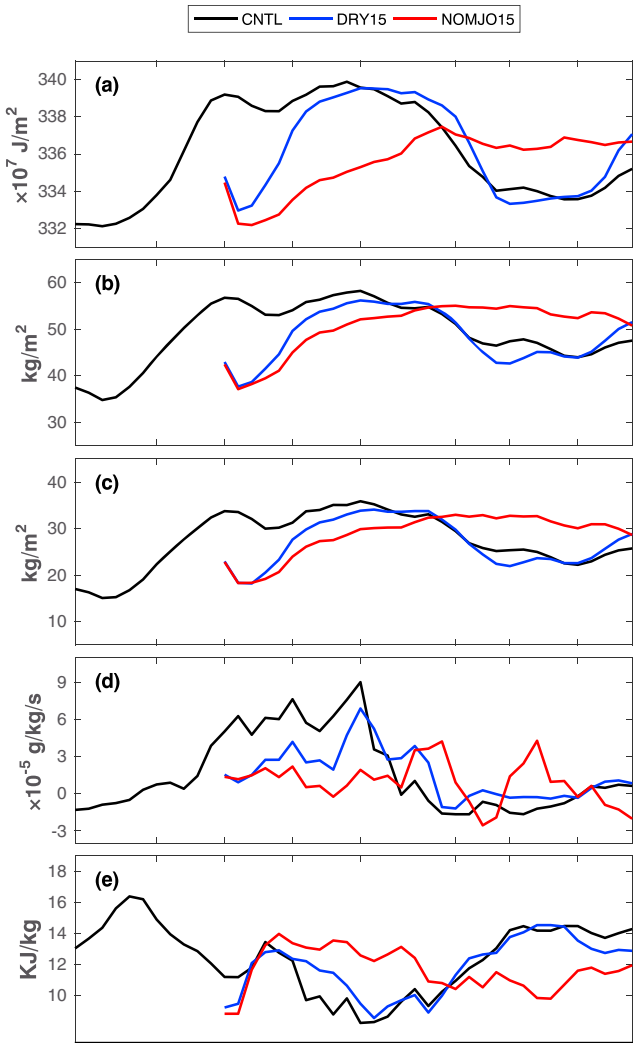

Figure 3. Time evolutions of the (a) column-integrated moist static energy, (b) column-integrated water vapor, (c) column-integrated water vapor above 850 hPa, (d) 850-hPa moisture convergence associated with the converging winds, and (e) moist static energy difference between 1,000 and 500 hPa averaged over the SR from CNTL, DRY15, and NOMJO15. A 3-day moving average is applied to all the time series.

converging winds ($-Q_v\frac{\partial U}{\partial X}-Q_v\frac{\partial V}{\partial y}$) can be found over the region (Figure 3d). Hence, moderately deep convection is triggered and moistens the middle troposphere efficiently (Figure S1). The moisture advection term ($-U\frac{\partial Q_v}{\partial X}-V\frac{\partial Q_v}{\partial y}$) is much weaker when compared to the moisture convergence associated with the converging winds at low levels (not shown here). It shows that the low-level dynamical convergence is more important than the low-level moisture advection in triggering the moderately deep convention. The MSE difference between 1,000 and 500 hPa decreases during 10–15 October (Figure 3e), which implies that the moderately deep convection transports energy from the lower troposphere to the middle troposphere. Accompany with the enhanced convective activity, the low-level moisture convergence and the moisture content above 850 hPa also peak near 25 October, while the MSE difference between 1,000 and 500 hPa reaches its minimum (Figures 3c–3e). After 1 November, the SR is occupied by the MJO suppress phase. The column-integrated MSE, column-integrated water vapor, and low-level moisture convergence all decrease over the SR (Figures 3a–3d), while the MSE difference between 1,000 and 500 hPa increases (Figure 3e).

In DRY15, the column-integrated MSE and water vapor quickly increase from 16 October and reaches a similar value to that in CNTL around 25 October (Figures 3a and 3b). The increase of the column-integrated MSE and water vapor corresponds to an enhancement of low-level moisture convergence associated with the converging winds (Figure 3d), which induces a moistening above the lower troposphere (Figure 3c). However, in NOMJO15, the low-level moisture convergence during 15–25 October is much weaker than that in DRY15 (Figure 3d). As a result, less moderately deep convection is triggered over the SR (Figure S2j), and a drier troposphere can be found in NOMJO15 (Figures 3b and 3c). The peaks of the column-integrated MSE and water vapor around 25 October also disappeared in NOMJO15 (Figures 3a–3c). The MSE difference between 1,000 and 500 hPa increases during 15–18 October in both DRY15 and NOMJO15. It is closely related to the moistening of the lower troposphere by the shallow cumuli (Figure 2). The value of the MSE difference between 1,000 and 500 hPa decreases considerably after 18 October in DRY15 and reaches a similar minimum as that in CNTL around 25 October. However, the decrease of the MSE difference after 18 October in NOMJO15 is much weaker than that in DRY15, with no minimum that can be found around 25 October. It demonstrates that the low-level dynamical convergence associated with the circumnavigating MJO mode is important to preconditioning moistening and convective initiation of the MJO event. The difference of the low-level moisture convergence associated with the dynamical converging winds between DRY15 and NOMJO15 (~2×10^{-5} g/kg/s at 850 hPa; Figure 3d) results in 4.7 kg/m^2 difference in column-integrated water vapor (mainly contributed by changes of the water vapor content above 850 hPa) during 15–20 October (Figures 3a–3c).

The DRY15 also shows a similar MJO suppress phase as CNTL around 5–10 November, with the column-integrated MSE, the column-integrated water vapor, and the low-level moisture convergence decrease, but the MSE difference increases over the SR. However, all these features disappeared in NOMJO15 (Figure 3).

4. Concluding Remarks

Using a regional scale convection-permitting model, this study demonstrates the relative roles of preconditioning moistening and global circumnavigating mode on the convective initiation of the October 2011

MJO event that occurred during DYNAMO. The control simulation shows that there is a rapid transition period before the MJO active phase in this MJO event, when the middle troposphere is rapidly moistened by the widespread moderately deep convection.

A series of sensitivity experiments has been conducted in this study to show that the gradual (around 2 weeks) moistening process associated with surface fluxes proposed by the discharge-recharge hypothesis cannot accurately describe the timing and location of the MJO convective initiation (AVG20). The result is consistent with many other earlier studies (e.g., Lin et al., 2007; Ray et al., 2009). The rapid moistening in the middle troposphere before the MJO active phase is crucial to the MJO-associated rainfall and deep convection (DRY20). It only takes a few days for the formation of the widespread moderately deep convection, which moistens the middle troposphere after the MJO suppressed phase (DRY15). The large-scale circulations, especially vertical motion, associated with the global circumnavigating mode are responsible for the rapid preconditioning humidification in the middle troposphere and the triggering of deep convection during the MJO active phase (NOMJO15).

This study has focused on the October DYNAMO MJO event; more MJO events should be investigated in the future to assess the robustness of these findings. Further, the current study does not preclude the possible influences of midlatitude disturbances on the MJO convective initiation (e.g., Li et al., 2015). More detailed studies are needed to clarify these midlatitude interactions and influences.

Acknowledgments
This research is sponsored by National Science Foundation grant 1712290. Discussions with James Ruppert and many other were beneficial. The authors acknowledge the Texas Advanced Computing Center (TACC) at the University of Texas at Austin for providing computing and storage resources that have contributed to the research results reported within this paper. All data presented and the filtering codes can be downloaded from http://hfip.psu.edu/xzc55/MJO.tar.gz. The authors thank the two anonymous reviewers for their detailed and valuable suggestions.

References

Ajayamohan, R. S., Khouider, B., & Majda, A. J. (2013). Realistic initiation and dynamics of the Madden-Julian Oscillation in a coarse resolution aquaplanet GCM. *Geophysical Research Letters*, *40*, 6252–6257. https://doi.org/10.1002/2013GL058187

Benedict, J. J., & Randall, D. A. (2007). Observed characteristics of the MJO relative to maximum rainfall. *Journal of the Atmospheric Sciences*, *64*(7), 2332–2354. https://doi.org/10.1175/jas3968.1

Bergman, J. W., Hendon, H. H., & Weickmann, K. M. (2001). Intraseasonal air–sea interactions at the onset of El Niño. *Journal of Climate*, *14*(8), 1702–1719. https://doi.org/10.1175/1520-0442(2001)014<1702:iasiat>2.0.co;2

Bladé, I., & Hartmann, D. L. (1993). Tropical intraseasonal oscillations in a simple nonlinear model. *Journal of the Atmospheric Sciences*, *50*(17), 2922–2939. https://doi.org/10.1175/1520-0469(1993)050<2922:tioias>2.0.co;2

Chen, X., Pauluis, O. M., & Zhang, F. (2018). Atmospheric overturning across multiple scales of an MJO event during the CINDY/DYNAMO campaign. *Journal of the Atmospheric Sciences*, *75*(2), 381–399. https://doi.org/10.1175/jas-d-17-0060.1

Chi, Y., Zhang, F., Li, W., He, J., & Guan, Z. (2015). Correlation between the onset of the East Asian subtropical summer monsoon and the eastward propagation of the Madden–Julian Oscillation. *Journal of the Atmospheric Sciences*, *72*(3), 1200–1214. https://doi.org/10.1175/jas-d-14-0038.1

Emanuel, K. A. (1987). An air-sea interaction model of intraseasonal oscillations in the tropics. *Journal of the Atmospheric Sciences*, *44*(16), 2324–2340. https://doi.org/10.1175/1520-0469(1987)044<2324:aasimo>2.0.co;2

Fu, X., Lee, J.-Y., Hsu, P.-C., Taniguchi, H., Wang, B., Wang, W., & Weaver, S. (2013). Multi-model MJO forecasting during DYNAMO/CINDY period. *Climate Dynamics*, *41*(3-4), 1067–1081. https://doi.org/10.1007/s00382-013-1859-9

Gahtan, J., & Roundy, P. (2018). Extratropical influence on 200 hPa easterly acceleration over the western Indian Ocean preceding Madden-Julian Oscillation convective onset. *Journal of the Atmospheric Sciences*. https://doi.org/10.1175/jas-d-18-0069.1

Hohenegger, C., & Stevens, B. (2013). Preconditioning deep convection with cumulus Congestus. *Journal of the Atmospheric Sciences*, *70*(2), 448–464. https://doi.org/10.1175/jas-d-12-089.1

Hoskins, B. (2013). The potential for skill across the range of the seamless weather-climate prediction problem: A stimulus for our science. *Quarterly Journal of the Royal Meteorological Society*, *139*(672), 573–584. https://doi.org/10.1002/qj.1991

Hsu, H.-H., Hoskins, B. J., & Jin, F.-F. (1990). The 1985/86 intraseasonal oscillation and the role of the extratropics. *Journal of the Atmospheric Sciences*, *47*(7), 823–839. https://doi.org/10.1175/1520-0469(1990)047<0823:tioatr>2.0.co;2

Johnson, R. H., & Ciesielski, P. E. (2013). Structure and properties of Madden–Julian Oscillations deduced from DYNAMO sounding arrays. *Journal of the Atmospheric Sciences*, *70*(10), 3157–3179. https://doi.org/10.1175/jas-d-13-065.1

Johnson, R. H., Rickenbach, T. M., Rutledge, S. A., Ciesielski, P. E., & Schubert, W. H. (1999). Trimodal characteristics of tropical convection. *Journal of Climate*, *12*(8), 2397–2418. https://doi.org/10.1175/1520-0442(1999)012<2397:tcotc>2.0.co;2

Kemball-Cook, S. R., & Weare, B. C. (2001). The onset of convection in the Madden–Julian Oscillation. *Journal of Climate*, *14*(5), 780–793. https://doi.org/10.1175/1520-0442(2001)014<0780:toocit>2.0.co;2

Kikuchi, K., & Takayabu, Y. N. (2003). Equatorial circumnavigation of moisture signal associated with the Madden-Julian Oscillation (MJO) during boreal winter. *Journal of the Meteorological Society of Japan. Ser. II*, *81*(4), 851–869. https://doi.org/10.2151/jmsj.81.851

Kikuchi, K., & Takayabu, Y. N. (2004). The development of organized convection associated with the MJO during TOGA COARE IOP: Trimodal characteristics. *Geophysical Research Letters*, *31*, L10101. https://doi.org/10.1029/2004GL019601

Knutson, T. R., & Weickmann, K. M. (1987). 30–60 day atmospheric oscillations: Composite life cycles of convection and circulation anomalies. *Monthly Weather Review*, *115*(7), 1407–1436. https://doi.org/10.1175/1520-0493(1987)115<1407:daoclc>2.0.co;2

Lau, K.-M., & Peng, L. (1987). Origin of low-frequency (intraseasonal) oscillations in the tropical atmosphere. Part I: Basic theory. *Journal of the Atmospheric Sciences*, *44*(6), 950–972. https://doi.org/10.1175/1520-0469(1987)044<0950:oolfoi>2.0.co;2

Li, T., Zhao, C., Hsu, P.-c., & Nasuno, T. (2015). MJO initiation processes over the tropical Indian Ocean during DYNAMO/CINDY2011. *Journal of Climate*, *28*(6), 2121–2135. https://doi.org/10.1175/jcli-d-14-00328.1

Lin, H., Brunet, G., & Derome, J. (2007). Intraseasonal variability in a dry atmospheric model. *Journal of the Atmospheric Sciences*, *64*(7), 2422–2441. https://doi.org/10.1175/jas3955.1

Lorenz, D. J., & Hartmann, D. L. (2006). The effect of the MJO on the North American Monsoon. *Journal of Climate*, *19*(3), 333–343. https://doi.org/10.1175/jcli3684.1

Ma, D., & Kuang, Z. (2016). A mechanism-denial study on the Madden-Julian Oscillation with reduced interference from mean state changes. *Geophysical Research Letters*, *43*, 2989–2997. https://doi.org/10.1002/2016GL067702

Madden, R. A., & Julian, P. R. (1971). Detection of a 40–50 day oscillation in the zonal wind in the tropical Pacific. *Journal of the Atmospheric Sciences*, *28*(5), 702–708. https://doi.org/10.1175/1520-0469(1971)028<0702:doadoi>2.0.co;2

Madden, R. A., & Julian, P. R. (1972). Description of global-scale circulation cells in the tropics with a 40–50 day period. *Journal of the Atmospheric Sciences*, *29*(6), 1109–1123. https://doi.org/10.1175/1520-0469(1972)029<1109:dogscc>2.0.co;2

Maloney, E. D., & Hartmann, D. L. (2001). The Madden–Julian Oscillation, barotropic dynamics, and North Pacific tropical cyclone formation. Part I: Observations. *Journal of the Atmospheric Sciences*, *58*(17), 2545–2558. https://doi.org/10.1175/1520-0469(2001)058<2545:tmjobd>2.0.co;2

Matthews, A. J. (2008). Primary and successive events in the Madden–Julian Oscillation. *Quarterly Journal of the Royal Meteorological Society*, *134*(631), 439–453. https://doi.org/10.1002/qj.224

Nasuno, T., Li, T., & Kikuchi, K. (2015). Moistening processes before the convective initiation of Madden–Julian Oscillation events during the CINDY2011/DYNAMO period. *Monthly Weather Review*, *143*(2), 622–643. https://doi.org/10.1175/mwr-d-14-00132.1

Peatman, S. C., Matthews, A. J., & Stevens, D. P. (2014). Propagation of the Madden–Julian Oscillation through the Maritime Continent and scale interaction with the diurnal cycle of precipitation. *Quarterly Journal of the Royal Meteorological Society*, *140*(680), 814–825. https://doi.org/10.1002/qj.2161

Powell, S. W. (2016). Updraft buoyancy within and moistening by cumulonimbi prior to MJO convective onset in a regional model. *Journal of the Atmospheric Sciences*, *73*(7), 2913–2934. https://doi.org/10.1175/jas-d-15-0326.1

Powell, S. W., & Houze, R. A. (2013). The cloud population and onset of the Madden-Julian Oscillation over the Indian Ocean during DYNAMO-AMIE. *Journal of Geophysical Research: Atmospheres*, *118*, 11,979–11,995. https://doi.org/10.1002/2013JD020421

Powell, S. W., & Houze, R. A. (2015a). Effect of dry large-scale vertical motions on initial MJO convective onset. *Journal of Geophysical Research: Atmospheres*, *120*, 4783–4805. https://doi.org/10.1002/2014JD022961

Powell, S. W., & Houze, R. A. (2015b). Evolution of precipitation and convective echo top heights observed by TRMM radar over the Indian Ocean during DYNAMO. *Journal of Geophysical Research: Atmospheres*, *120*, 3906–3919. https://doi.org/10.1002/2014JD022934

Rauniyar, S. P., & Walsh, K. J. E. (2011). Scale interaction of the diurnal cycle of rainfall over the maritime continent and Australia: Influence of the MJO. *Journal of Climate*, *24*(2), 325–348. https://doi.org/10.1175/2010jcli3673.1

Ray, P., & Li, T. (2013). Relative roles of circumnavigating waves and extratropics on the MJO and its relationship with the mean state. *Journal of the Atmospheric Sciences*, *70*(3), 876–893. https://doi.org/10.1175/jas-d-12-0153.1

Ray, P., Zhang, C., Dudhia, J., & Chen, S. S. (2009). A numerical case study on the initiation of the Madden–Julian Oscillation. *Journal of the Atmospheric Sciences*, *66*(2), 310–331. https://doi.org/10.1175/2008jas2701.1

Redelsperger, J.-L., Parsons, D. B., & Guichard, F. (2002). Recovery processes and factors limiting cloud-top height following the arrival of a dry intrusion observed during TOGA COARE. *Journal of the Atmospheric Sciences*, *59*(16), 2438–2457. https://doi.org/10.1175/1520-0469(2002)059<2438:rpaflc>2.0.co;2

Ruppert, J. H., & Johnson, R. H. (2015). Diurnally modulated cumulus moistening in the preonset stage of the Madden–Julian Oscillation during DYNAMO. *Journal of the Atmospheric Sciences*, *72*(4), 1622–1647. https://doi.org/10.1175/jas-d-14-0218.1

Skamarock, W., Klemp, J., Dudhia, J., Gill, D., Barker, D., Duda, M., et al. (2008). A Description of the advanced research WRF version 3 (2008) NCAR technical note, *Boulder*, *CO*.

Taraphdar, S., Zhang, F., Leung, L. R., Chen, X., & Pauluis, O. M. (2018). MJO affects the monsoon onset timing over the Indian region. *Geophysical Research Letters*, *45*, 10,011–10,018. https://doi.org/10.1029/2018GL078804

Tyrrell, G. C., Karoly, D. J., & McBride, J. L. (1996). Links between tropical convection and variations of the extratropical circulation during TOGA COARE. *Journal of the Atmospheric Sciences*, *53*(18), 2735–2748. https://doi.org/10.1175/1520-0469(1996)053<2735:lbtcav>2.0.co;2

Wang, S., Sobel, A. H., Zhang, F., Sun, Y. Q., Yue, Y., & Zhou, L. (2015). Regional Simulation of the October and November MJO Events Observed during the CINDY/DYNAMO Field Campaign at Gray Zone Resolution. *Journal of Climate*, *28*, 2097–2119. https://doi.org/10.1175/JCLI-D-14-00294.1

Wheeler, M., & Kiladis, G. N. (1999). Convectively coupled equatorial waves: Analysis of clouds and temperature in the wavenumber–frequency domain. *Journal of the Atmospheric Sciences*, *56*(3), 374–399. https://doi.org/10.1175/1520-0469(1999)056<0374:ccewao>2.0.co;2

Yano, J.-I., & Emanuel, K. (1991). An improved model of the equatorial troposphere and its coupling with the stratosphere. *Journal of the Atmospheric Sciences*, *48*(3), 377–389. https://doi.org/10.1175/1520-0469(1991)048<0377:aimote>2.0.co;2

Yoneyama, K., Zhang, C., & Long, C. N. (2013). Tracking pulses of the Madden–Julian Oscillation. *Bulletin of the American Meteorological Society*, *94*(12), 1871–1891. https://doi.org/10.1175/bams-d-12-00157.1

Zhang, C. (2005). Madden-Julian Oscillation. *Reviews of Geophysics*, *43*, RG2003. https://doi.org/10.1029/2004RG000158

Zhang, F., Taraphdar, S., & Wang, S. (2017). The role of global circumnavigating mode in the MJO initiation and propagation. *Journal of Geophysical Research: Atmospheres*, *122*, 5837–5856. hts://doi.org/10.1002/2016JD025665